JOURNAL OF MATERIALS SCIENCE **39** (2004) 67–71

Effects of deformation on hydrogen degradation in a duplex stainless steel

S. S. CHEN
Institute of Materials Engineering, National Taiwan Ocean University, Keelung, Taiwan 20224, Republic of China

T. I. WU
Department of Materials Engineering, Tatung University, Taipei, Taiwan 10451, Republic of China

J. K. WU*
Institute of Materials Engineering, National Taiwan Ocean University, Keelung, Taiwan 20224, Republic of China
E-mail: A0055@mail.ntou.edu.tw

Hydrogen embrittlement of annealed, 20 and 40% cold worked 2205 duplex stainless steels has been evaluated using electrochemical permeation measurement, hydrogen microprint technique and tensile test in this study. Due to hydrogen transport in 2205 duplex stainless steel is mainly lattice diffusion in ferritic phase, more hydrogen distribution, higher permeation rate and effective diffusion in ferritic phase were detected. Hydrogen trapping and mechanical property effects were studied for cold worked specimens. Fractographic investigation revealed that hydrogen absorption promoted transgranular fracture in cold worked specimens. These results exhibits that the cold worked duplex stainless steels are more susceptible to hydrogen embrittlement.

1. Introduction

The duplex stainless steels are mixtures of austenite and ferrite. Their corrosion resistance, strength and toughness are in between those of the ferrite and austenite. They also have good ductility and weldability and are attractive materials for oil, gas and petrochemical industries. In order to meet the demands of industry, duplex stainless steel is inevitably deformed by different manufacturing and fabrication procedure and it is therefore important to choose a manufacturing route. Duplex stainless steels offer improved resistance to stress corrosion cracking compared to austenitic stainless steels [1–3], but the austenitic-ferritic duplex stainless steels should be considered susceptible to hydrogen embrittlement due to the higher diffusivity and permeation rate of hydrogen in the ferritic phase [4–6].

The present paper concerns the influence of cold deformation on hydrogen degradation of 2205 duplex stainless steel. The purpose of this paper is to report the results of the hydrogen diffusion, hydrogen distribution and fracture surface of annealed and cold worked 2205 duplex stainless steels by electrochemical permeation measurement, hydrogen microprint technique and tensile test.

2. Experimental procedure

The alloys used in this study were 2205 duplex stainless steels, and were analyzed and supplied by Gloria Material Technology Corporation (GMTC). Specimens were cut from alloy plate. The preparation of these specimens were homogenized at 1100°C for 1 h and followed by water quenching. The preparation of deformed specimens involved cold rolled to 20 and 40% reduction respectively. The chemical compositions of 2205 duplex stainless steel are list in Table I, and optical micrographs are shown in Fig. 1.

The instrumentation and procedures were similar to those described elsewhere [7]. The cathodic side, or hydrogen entry side, of the cell was galvanostatically polarized at a constant current density (20 $mA \cdot cm^{-2}$) in 0.05 M H_2SO_4 with 0.5 g/l As_2O_3 added as hydrogen recombination poison. The anodic side, or hydrogen exit side, of the cell was held at constant potential of 250 mV (SCE) in 0.1 M NaOH. The potentiostatic current gave a direct measure of the hydrogen flow rate. The cell assembly was immersed in a constant temperature bath maintained at 25 ± 1°C. Permeation specimens were fabricated to 40 × 30 × 1 mm sheets and then polished with grinding paper down to 1000 grit, finally finished with a thickness of 0.16–0.21 mm. The surfaces were rinsed with distilled water, cleaned ultrasonically in acetone, and dried quickly by warm air. The exit side of each specimen was electroplated with a thin nickel layer. The thickness of the nickel layer was 0.2 μm, so that the hydrogen permeation current density could be obtained correctly and the background current

*Author to whom all correspondence should be addressed.

TABLE I Chemical composition of 2205 duplex stainless steel

Element	C	Si	Mn	P	S	Ni	Cr	Mo	Cu	V	W	Al	Co	N
wt%	0.03	0.37	1.53	0.03	0.01	5.32	22.79	3.00	0.04	0.04	0.01	0.04	0.03	0.20

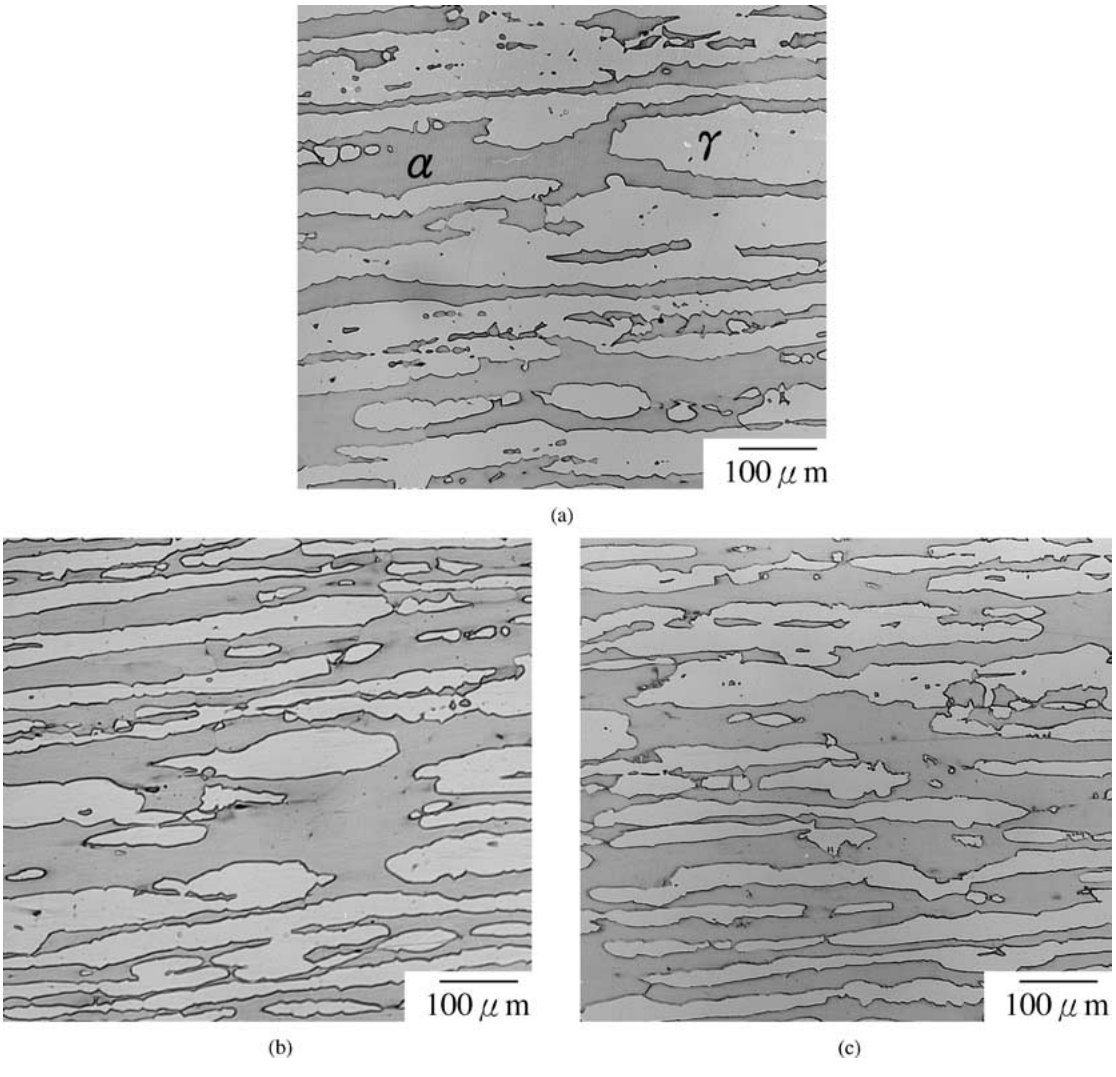

Figure 1 Optical micrographs of: (a) annealed, (b) CW 20% and (c) CW 40%.

density minimized. Both sides of the membrane were deoxygenated. Permeation transients were recorded on a strip chart recorder.

For this study the flux of hydrogen through the specimen was measured in terms of the steady-state current density, i_p^{∞}(mA·cm^{-2}), and was converted to the steady-state hydrogen permeation flux, J_{∞} (mol·m^{-2}·s^{-1}), according to

$$J_{\infty} = \frac{i_p^{\infty}}{nF} \tag{1}$$

where n is the number of electrons involved 1/mol and F is the Faraday's constant. The hydrogen permeation rate (mol·m^{-1}·s^{-1}) is defined by

$$J_{\infty}L = \frac{i_p^{\infty}}{nF}L \tag{2}$$

where L is the specimen thickness in mm. For diffusion as the rate-limiting step, the effective diffusivity, D_{eff} (m^2·s^{-1}) is related to the time lag, t_L (s), by [8]

$$D_{\text{eff}} = \frac{L^2}{6t_L} \tag{3}$$

Experimental set-up for hydrogen microprint technique is quite similar to that used for permeation measurement [9–11]. The cathodic charging side or hydrogen entry cell was also galvanostatically polarized at a constant charging current in 0.05 M $H_2SO_4$with 0.5 g/l As_2O_3. The hydrogen exit side was covered with liquid nuclear emulsion containing AgBr crystal as described by Overjero Garcia [12]. Before coating with nuclear emulsion, the specimen surface was polished down to 0.05 μm alumina, and etched in dilute aqua regia for metallographic preparation. During cathodic charging, hydrogen flux from the metal acted on the emulsion for the desired time causing the reduction of silver ions. Reactions in the exit side should be

mainly:

$$H^{\circ} + Ag^{+} \rightarrow H^{+} + Ag^{\circ} \quad (4)$$

After a designed cathodic charging time, the specimen was removed and placed into a fixing solution at room temperature, and then the specimen was washed with distilled water, dried and observed by scanning electron microscopy (SEM). Some blank specimens with the same preparation but without hydrogen charging were also analyzed.

ASTM E8 subsize tensile specimens with gage section of 25 × 6 × 1 mm were fabricated by EDM, and polished through 0.05 μm alumina. Tensile specimens were tested in air for the uncharged and cathodic charged conditions. The hydrogen charging was done in 0.05 M H_2SO_4 with 0.5 g/l As_2O_3 by making the specimen as a cathode. Platinum served as the counter electrode. A Luggin probe, with saturated calomel electrode and nitrogen gas dispersion, was inserted in this prepared solution. The tensile specimens were insulated with a stop-off coating except on the gauge section. For the precharging test, a specimen was charged with a constant current density (20 mA·cm^{-2}) for 5 days, then it was removed from the electrolyte, rinsed with distilled water, acetone, and dried with pressurized air. The specimen was then immediately strained to failure using a Shimadzu AG-250 KNG tensile testing machine. The strain rate adopted in this study was 5 × 10^{-5} s^{-1}. After completing the tensile test, the fracture surface was examined by scanning electron microscopy.

3. Results and discussion

3.1. Permeation test

Permeation rate and diffusivity of the duplex stainless steel at 25°C with a constant charging current density (20 mA · cm^{-2}) from permeation measurement are listed in Table II. The effective diffusivity and permeation rate of 2205 duplex stainless steel are three orders lower than those of AISI 430 ferritic stainless steel [13], and much higher than the value extrapolated from high temperature gas phase measurement of austenitic stainless steel [14–16]. Effective diffusivity in 2205 stainless steels, which was reported 1.5 to 6.4 × 10^{-14} m^2·s^{-1} at room temperature by previously investigators [1, 6, 11]. The average effective diffusivity (2.2 × 10^{-14} m^2·s^{-1}) in our experiments is quite close to the previous report. The date also clearly show a decrease in D_{eff} but an increased in $J_{\infty}L$ as cold rolled percentage increased for annealed specimens. The value of D_{eff} is decreased with increasing cold work, is due to the more hydrogen trapping site

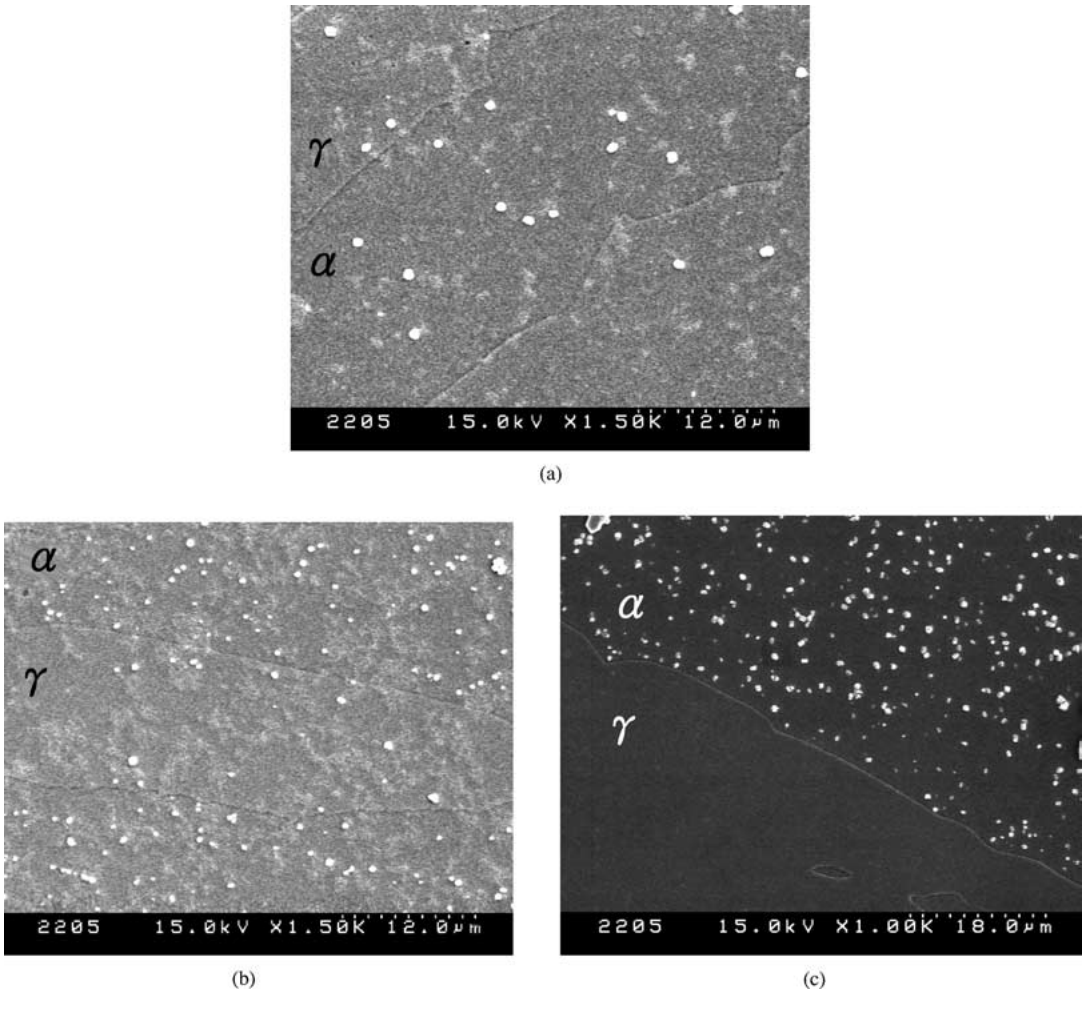

Figure 2 Specimen surface of: (a) annealed, (b) CW 20% and (c) CW 40% after cathodic charging with a constant current density (20 mA·cm^{-2}) in 0.05 M H_2SO_4 with 0.5 g/l As_2O_3 at 25°C for 7 days.

TABLE II The permeation data of 2205 duplex stainless steel

2205 DSS	D_{eff} ($m^2 \cdot s^{-1}$)	$J_\infty L$ (mol $H \cdot m^{-1} \cdot s^{-1}$)
Annealed	2.2×10^{-14}	9.0×10^{-11}
CW 20%	1.9×10^{-14}	9.6×10^{-11}
CW 40%	1.7×10^{-14}	1.1×10^{-10}

resulting from dislocations and deformation-induced microvoids [17, 18]. Cold work increases the $J_\infty L$, this effect has been explained by short-circuit diffusion paths down dislocations networks as well as by low energy trapping of hydrogen to dislocation [19, 20].

3.2. Hydrogen microprint technique

It was observed that reduced silver grains by hydrogen are gradually increased on specimen surfaces after cathodic charging with a constant current density at room temperature. Due to hydrogen permeation rate and effective diffusivity in ferritic phase is higher than in austenitic phase of duplex stainless steel, and more silver grains can be observed on ferritic phase, after cathodic charging time (7 days) in Fig. 2. The permeation rate and effective diffusivity of hydrogen is strongly affected by diffusion path and trapping sites. No silver grains are visible at grain boundaries in microprint technique; the hydrogen transport in 2205 duplex stainless steel is mainly in lattice diffusion through ferritic phase. More silver grains are observed in 40% cold worked specimen with high dislocation density in Fig. 2c. The fine silver grains located on specimen surface were analyzed and confirmed by EDX. Microprint technique is well developed to observe hydrogen distribution, and detects the hydrogen diffusion paths and trapping sites accurately. More silver grains reduced during shorter cathodic charging time, which means higher hydrogen permeation rate and diffusivity in ferritic phase.

3.3. Tensile testing

Tensile properties of hydrogen charged and uncharged specimens are listed in Table III. The tensile data show a significant loss in ductility with cathodic charging for 5 days. The uncharged specimens were mainly ductile fracture as shown in Figs 3–5a. The fractography of precharged specimens in Figs 3–5b show a mixture of facet cleavage fracture in ferritic phase and cleavage fracture associated with plastic deformation in austenitic phase. Some of hydrogen-assisted secondary cracks at the fracture surface were also observed in cold worked specimen, shown in Figs 4 and 5b respectively.

TABLE III Tensile properties of 2205 duplex stainless steel

2205 DSS	Test environment	UTS (MPa)	Elongation (%)
Annealed	Uncharged	788	38.2
	Precharged	734	8.35
CW 20%	Uncharged	1096	10.9
	Precharged	1069	1.92
CW 40%	Uncharged	1248	5.67
	Precharged	1232	2.36

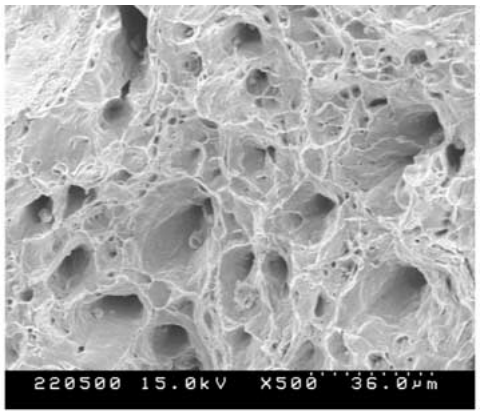

(a)

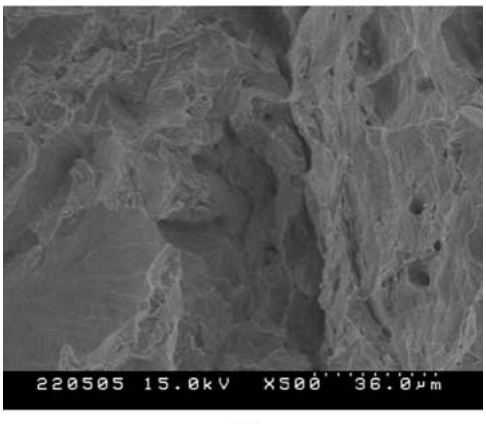

(b)

Figure 3 Fracture surface of annealed specimen: (a) uncharged and (b) 5 days cathodic charged.

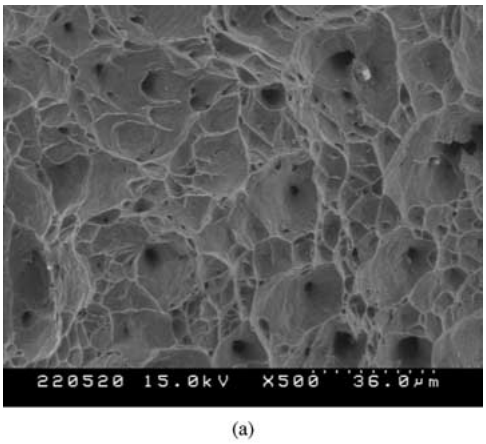

(a)

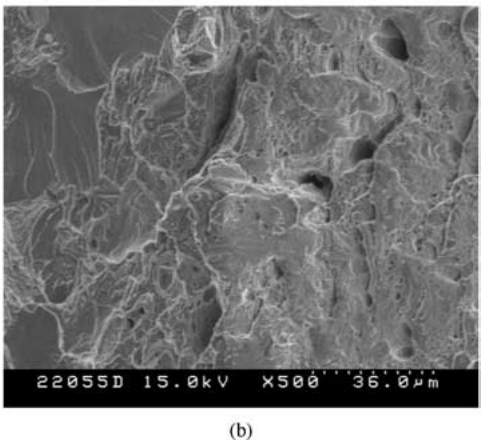

(b)

Figure 4 Fracture surface of 20% cold worked specimen: (a) uncharged and (b) 5 days cathodic charged.

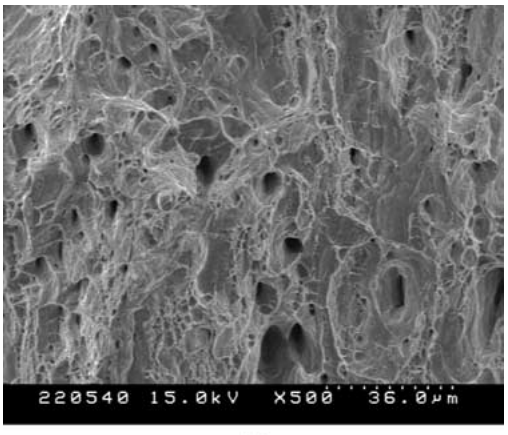

(a)

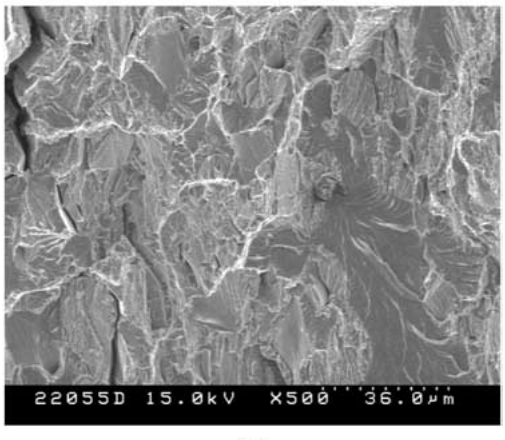

(b)

Figure 5 Fracture surface of 40% cold worked specimen: (a) uncharged and (b) 5 days cathodic charged.

These results can be explained as higher hydrogen diffusivity within ferritic grains and more hydrogen trapping sites in cold worked specimen with higher dislocation density. Strain and hydrogen-induced austenitic to martensitic transformation have not been observed, due to austenitic phase shows the less susceptibility in hydrogen environment and causes less deformation [21]. Fractographic examinations have revealed that hydrogen absorption promoted grain crack transgranularly through the ferritic phase, and rough stepwise cracking for the austenite. The cracking path of hydrogen precharged specimens can be concluded as a typical brittle cleavage in the ferritic phase, and then which induces a micro-crack in the austenitic grain crossing the ferritic/austenitic boundary. Finally, the crack propagates through the austenitic grain as reported in our previous investigation [11].

4. Conclusions

1. Hydrogen permeation rate and effective diffusivity in ferritic phase is higher than in austenitic phase of 2205 duplex stainless steel, and more hydrogen distribution on ferritic phase can be detected by hydrogen microprint technique.

2. The cold worked specimens also show lower effective diffusivity and higher permeation rate. The cold worked specimen is more susceptible to hydrogen degradation.

Acknowledgements

The authors are grateful for the support of this research by the National Science Council, Republic of China under Contract No. NSC 91-2216-E-019-008.

References

1. R. B. HUTCHINGS, A. TURNBULL and A. T. MAY, *Scr. Metall. Mater.* **25** (1991) 2657.
2. A. TURNBULL and A. J. GRIFFITHS, *British Corros. J.* **31** (1996) 39.
3. A. A. EL-YAZGI and D. HARDIE, *Corros. Sci.* **40** (1998) 909.
4. W. Y. WEI, C. H. TZENG and J. K. WU, *J. Mater. Sci. Lett.* **9** (1990) 1357.
5. H. L. ESCHBACH, F. GROSS and S. SCHULIEN, *Vacuum* **13** (1963) 543.
6. S. L. CHOU and W. T. TSAI, *Mater. Sci. Eng.* A **270** (1999) 219.
7. R. D. MCCRIGHT, Ph.D. Thesis, The Ohio State University, Columbus, OH, 1971.
8. J. CRANK, "The Mathematics of Diffusion" (Oxford University Press, 1977) p. 44.
9. W. C. LUU and J. K. WU, *Mater. Lett.* **24** (1995) 175.
10. *Idem.*, *Corros. Sci.* **38** (1996) 239.
11. W. C. LUU, P. W. LIU and J. K. WU, *ibid.* **44** (2002) 1783.
12. J. OVERJERO-GARCIA, *J. Mater. Sci.* **20** (1985) 2623.
13. C. H. TZENG, W. Y. WEI and J. K. WU, *Mater. Sci. Technol.* **5** (1989) 1236.
14. T. P. PERNG and C. J. ALTSTETTER, *Acta Metall.* **34** (1986) 1771.
15. *Idem.*, *ibid.* **35** (1988) 1251.
16. *Idem.*, *Metall. Trans.* **19A** (1988) 145.
17. S. X. XIE and J. P. HIRTH, *Corrosion—NACE* **38** (1982) 486.
18. A. J. KUMNICK and H. H. JOHNSON, *Metall. Trans.* **5** (1974) 1199.
19. S. M. LEE and J. Y. LEE, *ibid.* **17A** (1986) 181.
20. G. S. FRANKEL and R. M. LATANISION, *Metall. Trans.* **17** (1986) 861.
21. W. ZHENG and D. HARDIE, *Corrosion.* **47** (1991) 792.

Received 25 April
and accepted 25 August 2003